Wettability and thermal stability of fluorocarbon films deposited by deep reactive ion etching

Yan Xin Zhuang[a] and Aric Menon
MIC, Department of Micro and Nanotechnology, Technical University of Denmark, Building 345 east, DK-2800, Kgs. Lyngby, Denmark

(Received 8 October 2004; accepted 24 January 2005; published 21 April 2005)

Fluorocarbon films have low surface energy and can be used as antistiction coating for microelectromechanical systems. By using the passivation process in a deep reactive ion etcher, the fluorocarbon films can be deposited and integrated with other processes in the clean room. The properties such as wettability, surface energies, and thermal stability, have been investigated in detail. It has been found that the fluorocarbon films deposited have a static water contact angle of 109° and a surface energy around 14.5 mJ/m^2, whereas as-received and as-deposited single silicon, poly silicon, and silicon nitride have a much lower water contact angle and a higher surface energy. The fluorocarbon films keep their good hydrophobicity up to 300 °C, and the degradation temperature depends on the thickness of the fluorocarbon films. Decomposition happens at lower temperatures (100–300 °C) even though the decomposition rate is quite slow without affecting the contact angle. The decomposition mechanism at low temperatures (less than 300 °C) might be different from that at high temperatures. It has been shown that the fluorocarbon film deposited by a deep reactive ion etcher tool provides very high hydrophobicity, low surface energy, good thermal stability, and antiadhesion behavior for use in nanoimprinting lithography. © *2005 American Vacuum Society.* [DOI: 10.1116/1.1875232]

I. INTRODUCTION

Recently, fluorocarbon films have been widely investigated[1–9] due to their low dielectric constant, high hydrophobicity, low friction coefficient, high chemical inertness, and biocompatibility. Fluorocarbon films are very useful in microelectromechanical systems (MEMS) device, among other things, as antistiction and antiadhesion coating for suspended structures.[2–6] Among many deposition techniques, plasma polymerization technique is one of the most effective methods. It has been reported[6] that it is better to form fluorocarbon film in a field-free zone in view of quality and coverage of the film. C_2F_4,[1] C_4F_8,[2] C_4F_8/CH_4,[3] CHF_3, C_2F_6, C_4F_{10}, and other monomers have been used to form fluorocarbon films. It has been found that deposition rate and thermal stability of the fluorocarbon films depend on the fluorine-to-carbon ratio and substrate temperatures.[3,6] Up to now, most plasma deposition techniques are based on capacitively coupled plasma. There is little effort to characterize films deposited with a high-density inductively coupled plasma tool, especially with a deep reactive ion etcher (DRIE) developed by Surface Technology Systems (STS), UK. Ayón *et al.*[4] reported on the fluorocarbon films deposited with a DRIE. However, the thermal stability of the fluorocarbon films deposited is not reported. On the other hand, the thermal stability of fluorocarbon films is quite important in considering sensor packaging process, for long-term durability, and in nanoimprinting process. In this work, fluorocarbon films are deposited by the passivation process in deep reactive ion etching, where C_4F_8 is used as a monomer source, and their wettability and thermal stability are investigated by contact angle measurements, atomic force microscopy, and ellipsometry.

II. EXPERIMENTAL TECHNIQUES

Fluorocarbon films were deposited on *n*-(100) silicon wafers using a passivation process in STS DRIE tool, where C_4F_8 is used as a feed gas. After feeding C_4F_8 gas into the DRIE chamber, C_4F_8 is ionized between anode and cathode to form ions and free radicals such as CF_2, CF_3, CF, C_xF_y, etc., and then the radicals diffuse to the substrate and polymerize to form a fluorocarbon $(C_xF_y)_z$ film. Before deposition, the silicon wafers were given a buffered hydrofluoric acid (HF) dip followed by a 5 min water rinse and a spin dry afterwards. The deposition parameters, which were varied in DRIE, are C_4F_8 gas flow, coil power, and process time. In this investigation, the deposition temperature is 20 °C, the platen (bias) power is 20 W, and base pressure is 0.1 mTorr.

Thicknesses of fluorocarbon films were measured by variable angle spectroscopic ellipsometry. For each film sample, ellipsometric psi (ψ) and delta (Δ) angles were measured in step of 10 nm from wavelengths of 300–800 nm at incident angles of 70° and 80°. A three-layer model, i.e., (substrate)/(isotropic Cauchy film)/(air), is used to fit the data to get the thickness and refractive index by WVASE32™ software (developed by J. A. Woollam Co., Inc., USA). The fitting parameters were regressed to minimize the mean square error between the measured and modeled ψ and Δ.

Contact angle measurements were performed on contact angle meter DSA10 from Krüss GmbH, Germany equipped with automatic dispensing system and Framegrabber. The contact angles were determined by drop shape analysis soft-

[a]Electronic mail: yz@mic.dtu.dk

TABLE I. Surface tension of four test liquids (Ref. 10).

Test liquids	Total surface tension (mN/m)	Dispersive component (mN/m)	Polar component (mN/m)
DI-water	72.8	21.8	51
Di-iodomethane	50.8	50.8	0
Ethylene glycol	47.7	30.9	16.8
n-Hexadecane	27.6	27.6	0

ware. Test liquids were de-ionized (DI) water, diiodomethane (Aldrich 99%), and ethylene glycol (Aldrich 99.8%) and hexadecane (Fluka 99.9%) due to their wide range surface tensions and ratios of dispersive-to-polar components. The surface tensions of the four liquids[10] are given in Table I. Both static and dynamic contact angles have been measured. For static contact angles, the contact angle values were taken five seconds after depositing liquid droplet on the surface to allow droplet relaxation. At least ten measurements have been performed for each droplet. The static contact angle values reported are the average of at least three droplets. In order to measure the dynamic contact angles, test liquid is steadily pumped into a 2 μL initial sessile droplet until the base diameter of the droplet is larger than 6.5 mm, and then the liquid is steadily sucked from the droplet into the needle using a motor-driven syringe. The contact angles have been recorded approximately every second during the experiments. In order to eliminate the effect of dispensing needle, the advancing and receding contact angles are the average values for the droplet, whose base diameter is 8 times larger than the diameter of the dispensing needle.

A typical dynamic contact angle curve as a function of time is given in Fig. 1 together with the base diameter of the liquid droplet. The dynamic contact angle curve can be divided into four regions as separated by lines A, B and C. While steadily pumping the test liquid into the initial droplet, the dynamic contact angle keeps constant, and the base diameter increases. The advancing contact angle can be determined from the average value in this region. At line A, the liquid starts to be withdrawn into the syringe, and the base diameter of the droplet keeps constant even though the volume of the liquid droplet decreases with time. In this region (between lines A and B), the dynamic contact angle decreases with time. This region can be regarded as a transition region. From line B, the base diameter of the droplet decreases together with the volume of the droplet, while the dynamic contact angle nearly keeps constant, which can be considered as the receding contact angle. From line C, the contact angle decreases quickly with time; the needle might have some influence on the receding contact angle due to a small base diameter.

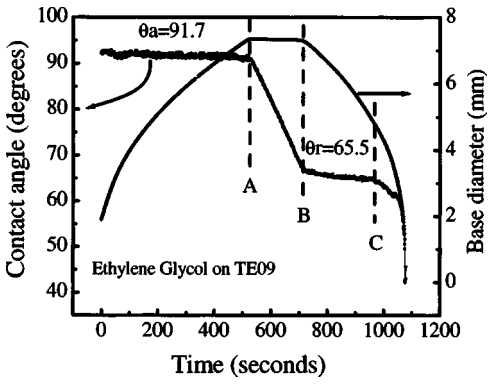

FIG. 1. Dynamic contact angle of ethylene glycol on fluorocarbon film TE09 and base diameter of the droplet as a function of time.

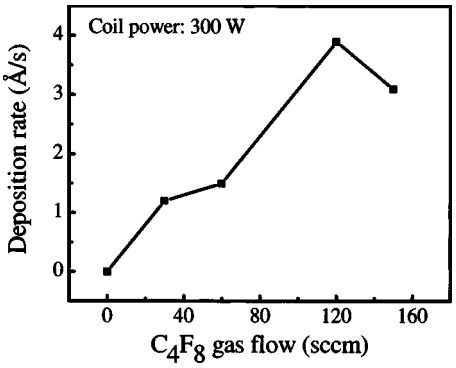

FIG. 2. Deposition rate as a function of C_4F_8 gas flow. Coil power is 300 W, platen power is 20 W, deposition temperature is 20 °C, and base pressure is 0.1 mTorr.

Surface topography and roughness were measured by atomic force microscopy (AFM) in contact mode using commercial silicon tips. Three samples with different thicknesses were chosen for studying thermal stability of fluorocarbon films. The samples were annealed at given temperatures in an oven in air for 10 min. The accuracy of the annealing temperatures is ±5 °C. The thermal stability is evaluated by the static contact angles of four test liquids and the thicknesses.

III. RESULTS AND DISCUSSIONS

A. Deposition of fluorocarbon films

In this investigation, the fluorocarbon films deposited are intended for antistiction and antiadhesion coating. Therefore, thicknesses of the fluorocarbon films deposited are not beyond 200 nm. The fluorocarbon films have been deposited on the fresh pretreated silicon substrates. Figure 2 gives the deposition rate of the fluorocarbon films as a function of C_4F_8 gas flow rate at a coil power of 300 W. The C_4F_8 gas flow was varied from 0 to 150 standard cm^3/min (sccm). It can be seen that the deposition rate increases with the flow rate until 120 sccm. Above 120 sccm, the plasma becomes unstable, and the deposition rate decreases. Figure 3 shows the relationship of the deposition rate with coil power at a C_4F_8 gas flow of 120 sccm. The coil power was changed from 0 to 600 W. It can be observed that the deposition rate increases linearly with the coil power in the range investigated.

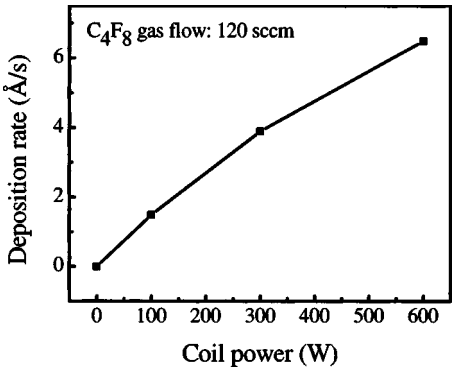

FIG. 3. Deposition rate as a function of coil power. C_4F_8 flow rate is 120 sccm, platen power is 20 W, deposition temperature is 20 °C, and base pressure is 0.1 mTorr.

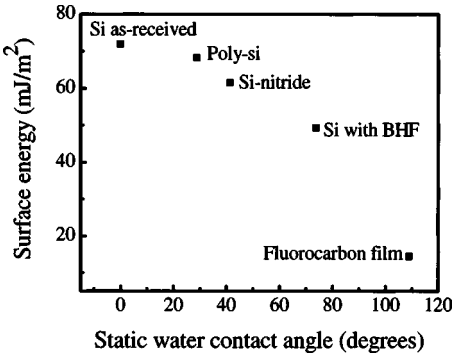

FIG. 4. Static water contact angles and surface energies of some common used MEMS materials and the fluorocarbon film.

B. Wettability and topography

The static water contact angles for all the fluorocarbon films deposited are 109±2°, which is high enough for avoiding adhesion and stiction in MEMS devices. It is well known that the contact angle of solid surfaces depends on the nature of materials and the topography. The same value of static water contact angles might indicate that the fluorocarbon films have similar topography. Three fluorocarbon films with different thicknesses are chosen for investigating dynamic contact angles, topography, and thermal stability. Among the three fluorocarbon films, the thinnest one is represented as TE10, the thickest one is identified as TE09, and the third one, TE02 has a thickness between them. The static and dynamic contact angles of the three selected fluorocarbon films are given in Table II together with their thicknesses. The wettability of the three fluorocarbon films is quite similar even though the thicknesses vary from 3.5 to 195 nm. The static contact angles of four test liquids are around 109° for water, 88° for di-iodomethane, 92° for ethylene glycol, and 56° for *n*-hexadecane. The water advancing contact angle, θ_{adv}, is between 119° and 121°, and the receding contact angle, θ_{rec}, is between 85° and 87°. The water contact angle hysteresis, i.e., the difference between the advancing and receding contact angles, has a similar value between 32.8° and 34.6° for the three films. The contact angle hysteresis is usually attributed to the chemical heterogeneity, the surface roughness, and the properties of test liquids. The similar water contact angle hysteresis means that the fluorocarbon films have similar roughness.

TABLE II. Thickness, contact angle (θ), and surface energies (γ) of three fluorocarbon films.

Sample	TE10	TE02	TE09
Thickness/mean square error (Å)	35.9/4.766	153.9/3.626	1951.8/12.49
$\theta_{static}(H_2O)\pm sd$[a] (deg)	109.0±0.9	108.8±1.4	109.3±0.7
$\theta_{static}(CH_2I_2)\pm sd$ (deg)	88.5±0.9	87.7±2.4	88.3±0.7
$\theta_{static}(C_2H_6O_2)\pm sd$ (deg)	91.1±0.4	93.4±0.7	92.2±0.8
$\theta_{static}(C_{16}H_{34})\pm sd$ (deg)	57.8±0.4	55.7±0.5	56.1±0.2
$\theta_{adv}(H_2O)\pm sd$ (deg)	119.5±0.5	121.8±0.5	119.5±0.7
$\theta_{rec}(H_2O)\pm sd$ (deg)	86.7±1.0	87.1±0.5	85.1±1.6
$\Delta\theta=\theta_{adv}-\theta_{rec}$ (deg)	32.8	34.6	34.4
γ_{sv} (mJ/m^2)	14.58	14.48	14.38
γ_{sv}^D (mJ/m^2)	14.55	14.48	14.35
γ_{sv}^P (mJ/m^2)	0.03	0.00	0.03

[a]Standard deviation.

Surface energy of the fluorocarbon films can be calculated from the contact angle data. According to Young's equation[11]

$$\gamma_{sv} = \gamma_{sl} + \gamma_{lv}\cos\theta, \tag{1}$$

where γ_{sv}, γ_{sl}, and γ_{lv} are surface energy of solid, interfacial tension between solid and liquid, and surface tension of liquid, respectively, and θ is the equilibrium contact angle of liquid on the solid surface. In order to get the surface energy from the contact angle measurements, it is necessary to know the relationship of γ_{sl} with γ_{sv} and γ_{lv}. Up to now, there are many assumptions for this relationship. In this article, we use Owens–Wendt–Rabel–Kaelble method[12–14] to evaluate the surface energy of various solid surfaces. In this method, the surface tension of each phase can be split into a polar and a dispersive fraction, i.e.,

$$\gamma_{sv} = \gamma_{sv}^D + \gamma_{sv}^P, \quad \gamma_{lv} = \gamma_{lv}^D + \gamma_{lv}^P. \tag{2}$$

The interfacial tension γ_{sl} can be calculated by the geometric mean equation:

$$\gamma_{sl} = \gamma_{sv} + \gamma_{lv} - 2\left(\sqrt{\gamma_{sv}^D\gamma_{lv}^D} + \sqrt{\gamma_{sv}^P\gamma_{lv}^P}\right), \tag{3}$$

where superscripts D and P represent the dispersive and polar components and the subscripts s, l, and v denote solid, liquid, and vapor phases, respectively. Combining Eq. (3) with Young's equation (1), the following linear equation can be obtained:

$$\frac{(1+\cos\theta)\gamma_{lv}}{2\sqrt{\gamma_{lv}^D}} = \sqrt{\gamma_{sv}^P}\sqrt{\frac{\gamma_{lv}^P}{\gamma_{lv}^D}} + \sqrt{\gamma_{sv}^D}. \tag{4}$$

Therefore, with at least two liquids with known values γ_{lv}, γ_{lv}^D, and γ_{lv}^P, the components of γ_{sv}^D and γ_{sv}^P can be determined from the intercept and the slope of the linear fit to the data. The total surface energy of solid can be calculated by summing the two components. The surface energies of the fluorocarbon films are calculated from the advancing contact

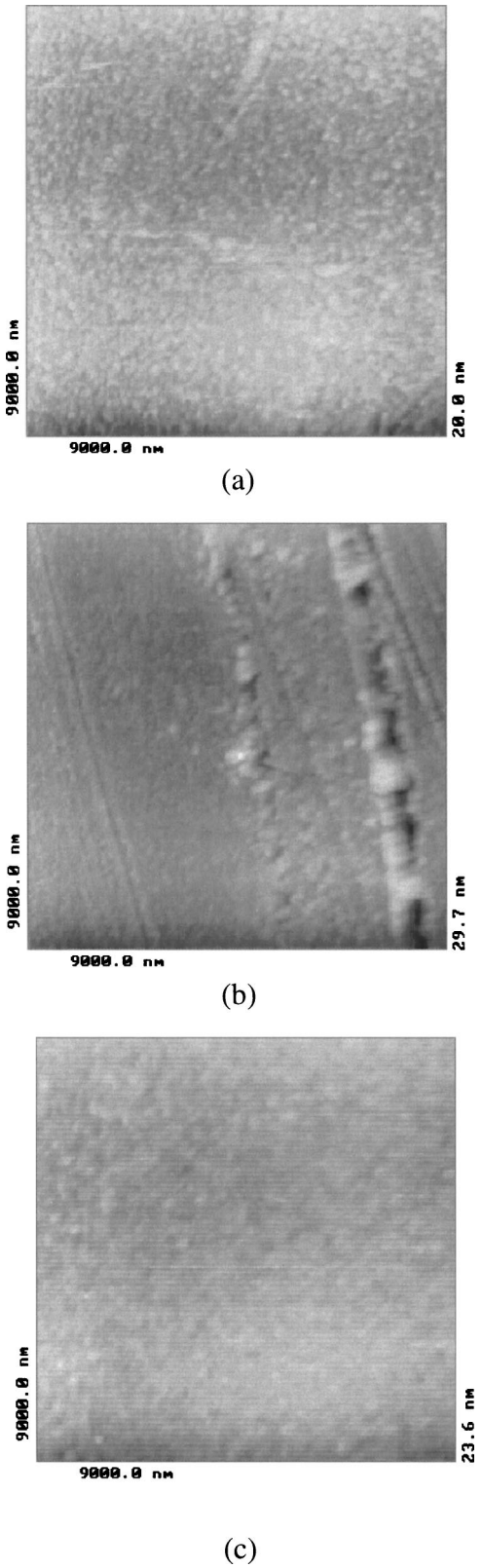

FIG. 5. AFM images of the fluorocarbon film (a) TE10, (b) TE02, and (c) TE09.

angle of four test liquids and are given in Table II. It can be seen that the fluorocarbon films have quite a low surface energy, approximately 14.5 mJ/m^2, and a nearly zero polar component of surface energy. As a reference, static water contact angles of some common used MEMS materials are measured, and their surface energies are calculated by the method stated previously. The results are shown in Fig. 4. As-received silicon, polysilicon and silicon nitride have a significantly lower water contact angle and a higher surface energy, and thereby a large tendency for stiction. The buffered HF cleaning can improve the hydrophobicity of silicon, but it is still not enough for antistiction coating. Fluorocarbon films deposited by DRIE have the highest water contact angle and lowest surface energy, and can be used for antistiction coating for those underlying materials. It has been reported that fluorocarbon films minimize stiction during the release process in nanoimprinting lithography.[15,16]

TABLE III. Thickness and roughness of three fluorocarbon films chosen.

Sample	TE10	TE02	TE09
Thickness/mean square error (Å)	35.9/4.766	153.9/3.626	1951.8/12.49
$R_a \pm$sd (nm)	1.0±0.4	1.4±0.4	1.0±0.3
rms±sd (nm)	1.2±0.4	1.8±0.4	1.3±0.3

The AFM images with 9×9 μm^2 scanning area for the three samples are given in Fig. 5. It can be observed that the topography of the three samples have no significant difference. Average roughness (R_a), root mean square (rms) roughness and their standard deviation (sd) of the three samples, which are calculated from five images for each sample, are shown in Table III. It can be seen that the three films have

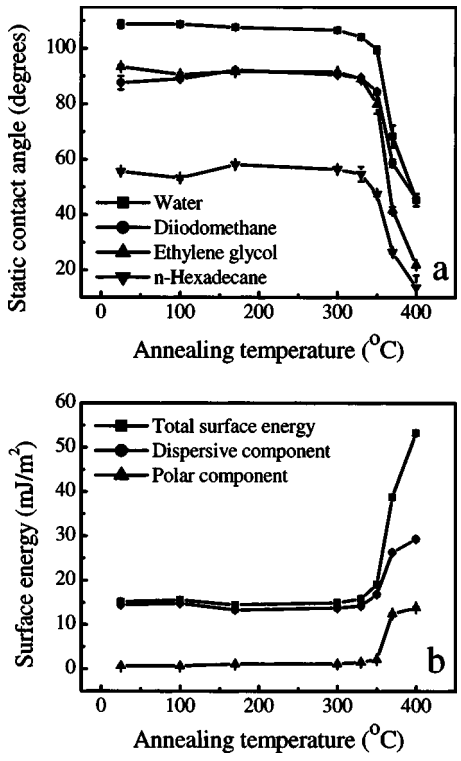

FIG. 6. (a) Static contact angles and (b) surface energy of the fluorocarbon film TE02 annealed at various temperatures in air for 10 min.

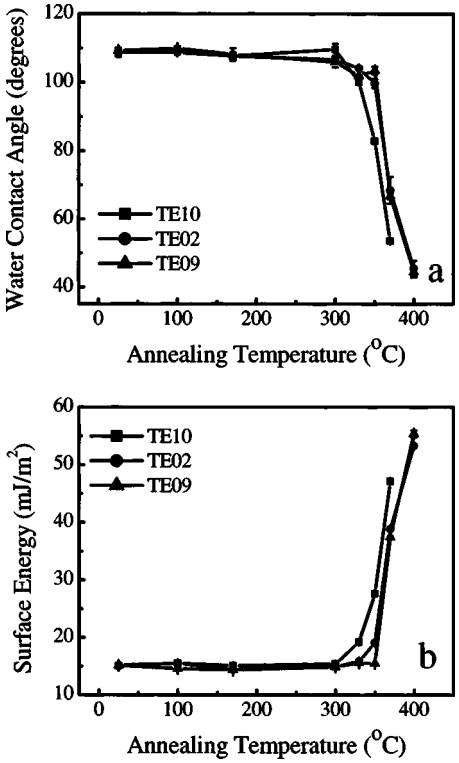

FIG. 7. (a) Static contact angles and (b) surface energy of the three fluorocarbon films as a function of annealing temperature. Annealing time is 10 min, in air.

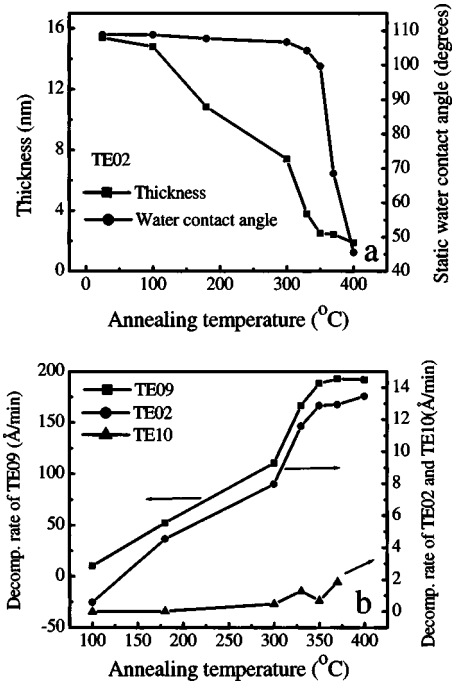

FIG. 8. (a) Static water contact angles and thickness of fluorocarbon film TE02, and (b) decomposition rates of the three films as a function of annealing temperatures. Annealing time is 10 min, in air.

similar R_a and rms roughness even though the thickness ranges from 3.6 to about 195 nm, which is in agreement with the conclusion from contact angle hysteresis.

C. Thermal stability

Thermal stability of the fluorocarbon films is estimated by the static contact angles and the surface energies calculated from the static contact angles. Figure 6 gives the static contact angles of four test liquids and the surface energy of fluorocarbon film TE02 annealed at various temperatures in air for 10 min. The static contact angles and surface energy of the film keep constant until 330 °C, then the static contact angles decrease quickly and the surface energy increases quickly with increasing annealing temperatures, indicating that the fluorocarbon film can be used as an antiadhesion and antistiction coating as long as the process temperature is less than 330 °C and process time is shorter than 10 min. Both dispersive and polar components of surface energy increase with annealing temperature after 330 °C, and provide similar contributions to enhance the total surface energy, indicating that no dominant component is responsible for the degradation of the fluorocarbon film. A similar trend has been found for the other two fluorocarbon films, TE09 and TE10. Figure 7 shows the static water contact angles and surface energies of all three fluorocarbon films as a function of annealing temperatures. It can be seen that the degradation temperature depends on the thicknesses of the initial films. The water contact angle starts to decrease at 300 °C for the film with an initial thickness of 3.6 nm (TE10), 330 °C for the film with an initial thickness of 15.4 nm (TE02), and 350 °C for the film with an initial thickness of 195.2 nm (TE09). This means that the degradation might be caused by decomposition of the fluorocarbon film.

The thickness of fluorocarbon film TE02 as a function of annealing temperatures is given in Fig. 8(a) together with their water contact angles. It can be seen that the thickness decreases even at 100 °C, indicating that the decomposition happens at low temperatures. The water contact angle keeps constant until 330 °C even though the thickness linearly decreases with the annealing temperatures. When the annealing temperature is higher than 300 °C, the thickness dramatically decreases, and the water contact angle decreases quickly with annealing temperatures, meaning that the decomposition mechanism at higher temperatures might be different from that at lower temperatures (less than 300 °C). Figure 8(b) shows the decomposition rates of the three films as a function of annealing temperature. It can be observed that the decomposition rates at a given temperature are quite different for the three samples. The reason for the thickness-dependent decomposition is unknown.

IV. CONCLUSIONS

The fluorocarbon films have been deposited on the silicon substrates by the inductively coupled plasma technique using the passivation process in a deep reactive ion etcher. The deposition rate reached a maximum at a C_4F_8 gas flow of 120 sccm when the coil power is 300 W, and the deposition rate linearly increased with the coil power in the range of 100–600 W at a C_4F_8 gas flow of 120 sccm. All the fluoro-

carbon films deposited have a water contact angle as high as 109°, a surface energy as low as 14.5 mJ/m^2, in which the polar component is nearly zero. The degradation temperature of the fluorocarbon films depends on the thickness. It has been found that the decomposition rate depends on the thickness. The decomposition occurs even at low temperature (100 °C). The mechanisms for the decomposition of fluorocarbon films at low and high annealing temperatures are different.

ACKNOWLEDGMENTS

The authors would like to thank Flemming Jensen for useful discussion of AFM results, and financial support from European Commission under Contract No. G1ST-CT–2002–50354.

[1]G. Cicala, A. Milella, F. Palumbo, P. Favia, and R. d'Agostino, Diamond Relat. Mater. **12**, 2020 (2003).
[2]K. Takahashi, T. Mitamura, K. Ono, Y. Setsuhara, A. Itoh, and K. Tachibana, Appl. Phys. Lett. **82**, 2476 (2003).
[3]Y. Matsumoto and M. Ishida, Sens. Actuators, A **83**, 179 (2000).
[4]A. A. Ayón, D. Z. Chen, R. Khanna, R. Braff, H. H. Sawin, and M. A. Schmidt, Mater. Res. Soc. Symp. Proc. **605**, 141 (2000).
[5]Y. Matusumot, K. Yoshida, and M. Ishida, Sens. Actuators, A **66**, 308 (1998).
[6]P. F. Man, B. P. Gogoi, and C. H. Mastrangelo, J. Microelectromech. Syst. **6**, 25 (1997).
[7]K. Shibagaki, T. Maeda, N. Takada, K. Sasaki, and K. Kadota, J. Vac. Sci. Technol. A **41**, 866 (2003).
[8]K. Takahashi, A. Itoh, T. Nakamur, and K. Tachibana, Thin Solid Films **374**, 303 (2003).
[9]S. Agraharam, D. W. Hess, P. A. Kohl, and S. A. B. Allen, J. Vac. Sci. Technol. A **17**, 3265 (1999).
[10]Krüss GmbH DSA I software database.
[11]A. W. Adamson and A. P. Gast, *Physical Chemistry of Surfaces*, 6th ed. (Wiley, New York, 1997).
[12]D. K. Owens and R. C. Wendt, J. Appl. Polym. Sci. **13**, 1741 (1969).
[13]D. H. Kaelble and K. C. Uy, J. Adhes. **2**, 50 (1970).
[14]W. Rabel, Farbe Lack **77**, 997 (1971).
[15]D. Nilsson, S. Jensen, and A. Menon, J. Micromech. Microeng. **13**, S57 (2003).
[16]T. Nielsen, D. Nilsson, F. Bundgaard, P. Shi, P. Szabo, O. Geschke, and A. Kristensen, J. Vac. Sci. Technol. B **22**, 1770 (2004).